10-2010

VLT Observations of NGC 1097's “Dog-Leg” Tidal Stream: Dwarf Spheroidals and Tidal Streams

P. Galianni
Universita del Salento

F. Patat
ESO European Southern Observatory

James L. Higdon
Georgia Southern University, jhigdon@georgiasouthern.edu

S. Mieske
ESO European Southern Observatory

P. Kroupa
Argelander Institut fur Astronomie

A&A 521, A20 (2010)
DOI: 10.1051/0004-6361/200913518

Astronomy & Astrophysics

VLT observations of NGC 1097's "dog-leg" tidal stream⋆

Dwarf spheroidals and tidal streams

P. Galianni[1], F. Patat[2], J. L. Higdon[3], S. Mieske[4], and P. Kroupa[5]

[1] Undergraduate student, Universita del Salento, via per Arnesano 1, 73100 Lecce, Italy
e-mail: pasquale.galianni@gmail.com
[2] ESO European Southern Observatory, Karl Schwarzschild str. 2, 85748 Garching bei Muenchen, Germany
[3] Department of Physics, Georgia Southern University, Statesboro, GA 30458, USA
[4] ESO European Southern Observatory, Alonso de Cordova, 3107 Vitacura, Santiago, Chile
[5] Argelander Institut für Astronomie, Auf dem Hügel 71, 53121 Bonn, Germany

Received 21 October 2009 / Accepted 1 June 2010

ABSTRACT

Aims. We investigate the structure and stellar population of two large stellar condensations (knots A & B) along one of the faint optical "jet-like" tidal streams associated with the spiral NGC 1097, with the goal of establishing their physical association with the galaxy and their origin.
Methods. We use the VLT/FORS2 to get deep V-band imaging and low-resolution optical spectra of two knots along NGC 1097's northeast "dog-leg" tidal stream. With this data, we explore their morphology and stellar populations.
Results. Spectra were obtained for eleven sources in the field surrounding the tidal stream. The great majority of them turned out to be background or foreground sources, but the redshift of knot A (and perhaps of knot B) is consistent with that of NGC 1097. Using the V-band image of the "dog-leg" tidal feature we find that the two knots match the photometric scaling relations of canonical dwarf spheroidal galaxies (dSph) very well. Spectral analysis shows that knot A is mainly composed of stars near G-type, with no signs of ongoing star formation. Comparing its spectrum with a library of high resolution spectra of galactic globular clusters (GCs), we find that the stellar population of this dSph-like object is most similar to intermediate to metal rich galactic GCs. We find moreover, that the tidal stream shows an "S" shaped inflection as well as a pronounced stellar overdensity at knot A's position. This suggests that knot A is being tidally stripped, and populating the stellar stream with its stars.
Conclusions. We have discovered that two knots along NGC 1097's northeast tidal stream share most of their spectral and photometric properties with ordinary dwarf spheroidal galaxies (dSph). Moreover, we find strong indications that the "dog-leg" tidal stream arises from the tidal disruption of knot A. Since it has been demonstrated that tidally stripping dSph galaxies need to loose most of their dark matter before starting to loose stars, we suggest that knot A is at present a CDM-poor object.

Key words. galaxies: dwarf – galaxies: interactions – galaxies: individual: NGC 1097 – galaxies : jets – globular clusters: individual: 47 Tucanae

1. Introduction

1.1. The nature of NGC 1097's optical "jet-like" tidal streams

NGC 1097's network of faint optical "jets" have puzzled astronomers since their discovery in the mid-1970s (Wolstencroft & Zealey 1975; Arp 1976; Lorre 1978). These early observations established their blue optical colors and lack of optical emission lines. The fact that all four appear to radiate from NGC 1097's Seyfert 1 nucleus (see Fig. 1 in Lorre 1978 and Fig. 1) led quite naturally to explanations involving AGN phenomena. However, the sensitive upper flux limits at 1.4 GHz set by Wolstencroft et al. (1984) with the Very Large Array (VLA) showed that the "jets" optical emission did not arise through the synchrotron process. Their observations could not exclude the possibility that the "jets" were dominated by thermal Bremsstrahlung emission from a $\approx 10^6$ K plasma (the high temperature is required to explain the absence of Hα emission set by Arp 1976). The same year, Carter et al. (1984, hereafter CAM) proposed a very different interpretation based on optical and near-infrared surface photometry of the two northern jets and the most prominent of several optical knots in the northeast jet first noted by Arp (1976) and Lorre (1978). The colors of the diffuse light in the northern jets (e.g., $B - R = 0.6 \pm 0.3$ and $B - H = 2.6 \pm 0.4$) are inconsistent with both thermal Bremsstrahlung and synchrotron emission. Instead, CAM proposed that the "jet-like" features are in fact composed of *stars*, similar to ordinary disk populations (≈G-type). These stars either: formed in situ from the cooling plasma of an ancient radio jet, were drawn out of NGC 1097's disk through a tidal interaction with its companion NGC 1097A, or represented the remains of a dwarf irregular or small spiral galaxy cannibalized by the much larger NGC 1097 (i.e., a minor merger). CAM went so far as to propose that the prominent optical knot near the northeast jet's abrupt right-angle bend (called the "dog-leg") might be what is left of the dwarf's tidally-stripped nucleus, given that its color ($B - R = 0.9 \pm 0.2$) is similar to that of late-type spiral nuclei. Wehrle et al. (1997) used

⋆ Based on observations made with ESO telescopes at Paranal Observatory in the observing program 66.B-0481 (G. Rupprecht/ H. Arp).

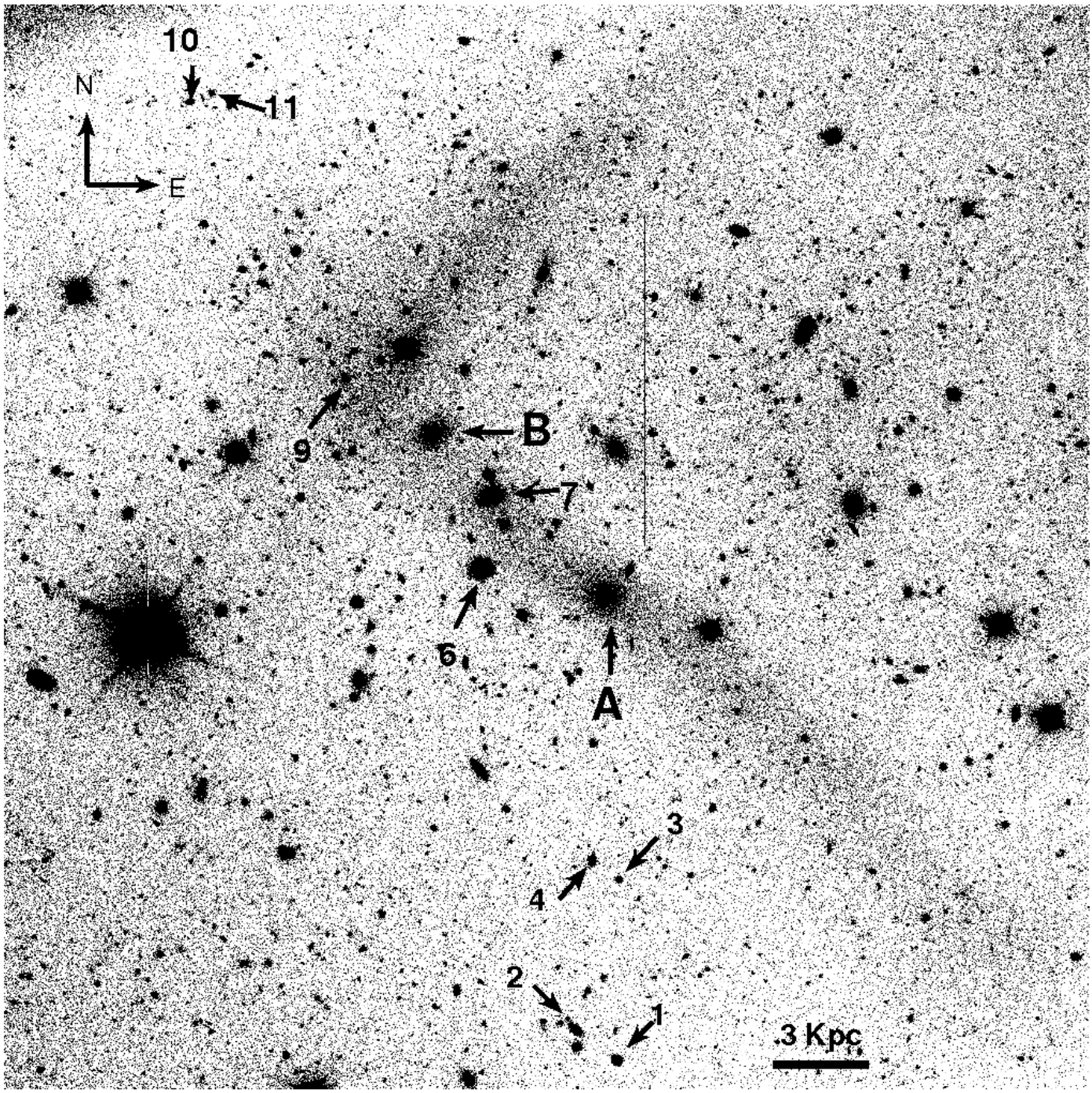

Fig. 1. FORS2/UT2 400 s Bessel V-band image of NGC 1097's northeast optical jet and "dog-leg". The targets observed spectoscopically with FORS2 are labeled as in Table 1. The figure covers $6.8' \times 6.8'$ with North at top and East to the left. NGC 1097 lies in direction of the bottom right corner of the picture.

VLA observations at 327 MHz to conclusively rule out the "jet-like" features being a network of ancient radio jets, and they concluded that NGC 1097's jets are nothing more than a set of unusual *tidal streams* created through multiple encounters with the small elliptical companion NGC 1097A. Since tidal streams, and especially *blue* tidal streams, are typically rich in neutral atomic hydrogen gas (HI), this opened the interesting possibility of using HI kinematics to explore their origin and evolution.

Higdon & Wallin (2003, hereafter HW) revived the "minor merger" interpretation for the tidal streams. Using the VLA in its most compact configuration, they found that all four tidal streams are extremely gas poor ($\Sigma_{\rm HI} < 0.06\ M_\odot\ {\rm pc}^{-2}, 3\sigma$). Given their blue color, they are unlike any tidal stream in the literature (cf. Hibbard et al. 2000; Higdon et al. 2006). The total lack of HI had additional implications: the stars could not have originated from the HI rich disk of NGC 1097, nor could they have been formed in situ from a cooling radio jet without unrealistic star formation efficiencies. HW proposed a scenario in which the tidal streams were formed by multiple passes of a gas rich dwarf galaxy through the center of the much more massive NGC 1097.

Their n-body simulations of such a capture produced features that strikingly resembled the four optical tidal streams, including the abrupt 90° bend of the dog-leg region (see their Figs. 12–14). The dwarf galaxy's ISM is swept out by ram pressure stripping during its initial pass through NGC 1097's disk, resulting in the creation of essentially gas free "jet-like" stellar streams. Within the HW picture, NGC 1097's optical tidal streams represents the late stages in the cannibalization of a small disk galaxy by a much larger spiral.

1.2. Structures in NGC 1097's northeast tidal stream

Arp (1976) and Lorre (1978) noted the presence of several optical knots near the northeast tidal feature's dog-leg region (see Figs. 1 and 3) that appeared too blue for background ellipticals, though with no redshifts available the possibility that they were background objects could not be ruled out. Wehrle et al. (1997) obtained 4000–7000 Å spectra of the two brightest knots using 1–2 h exposures with the CTIO 4 m Blanco telescope, and detected only weak continuum (after averaging over large wavelength bins) and no measurable line emission (e.g., $EW_{\mathrm{H}\alpha} < 15$ Å and $EW_{[\mathrm{O\ III}]}$, $EW_{\mathrm{H}\beta} < 30$ Å). Because of detector instabilities, the quality of their spectra was not sufficient to determine the nature of knots A & B. While it had yet to be established that the knots were in fact part of the northeast tidal stream, it was clear from their apparent lack of strong emission lines that neither were star forming dwarf galaxies or distant AGN. The existence of multiple knots are of particular interest, as they might represent ongoing structure formation in the tidal streams.

In this paper we analyze VLT/FORS2 spectra of five of the brightest optical knots in the northeast tidal stream. We show that the most prominent condensation, knot A, has the same redshift as the spiral NGC 1097, and argue that it is physically associated with the tidal stream. A second condensation, knot B, is also plausibly associated with the tidal feature[1].

The VLT observations are described in Sect. 2. In Sect. 3 we present the photometric and spectroscopic measurements of knots A & B, and discuss these findings and their implications in Sect. 4. Finally, we summarize our results in Sect. 5. Throughout this paper we have adopted the standard WMAP cosmology ($H_0 = 72 \pm 5$ km s^{-1} Mpc^{-1}; Spergel et al. 2003), which for NGC 1097's redshift ($z = 0.0042 \pm 0.0001$, e.g., Koribalski et al. 2004; Mathewson & Ford 1996) results in a luminosity distance D_{L} of 17 ± 2 Mpc and a linear scale of 84 pc/″.

2. VLT observations and data reduction

The observations were made at ESO-Paranal by G. Rupprecht and H. Arp (observing program 66.B-0481) on several runs: 7 October 2000 (ID 101443), 17 November 2000 (ID 103791), and 4 December 2000 (ID 103790). The data were kindly provided by Arp and Rupprecht. Optical spectra were obtained with the FORS2 imaging-spectrograph (1998), situated at the Cassegrain focus of the 8.2 m VLT Kueyen (UT2). The detector was a 2048 × 2048 TK2048EB4-1 thinned, backside illuminated CCD. The standard resolution collimator was used, providing an angular scale of 0.2″/pix and a field of view of 6.′8 × 6.′8. Grism GRIS_150I+27 was used, which provides a linear dispersion of 230 Å/mm and $\lambda/\Delta\lambda = 260 \pm 1.5$ (if coupled with a 1″ slit). Spectra covering the full 3300–1000 Å wavelength range were obtained in two stages: red spectra (6000–10 000 Å) using the OG590+32 filter as an order blocker, and blue spectra (3300–6600 Å) with no filter.

The observations were carried out in multi-object (MXU) mode, with twelve slits of varying widths (1″ to 2.5″) placed on the sky. One large slit was situated across the northeast tidal stream, one slit each was placed on knots A & B, six on field objects, and three on empty fields to measure sky emission. The integration time for the spectra was 30 min. Data reduction was routine, and standard procedures in IRAF were used to extract (*apall*), calibrate (*identify*, *calibrate*), and join (*scombine*) the red and blue spectrum for each slit. See Table 1 for the coordinates, photometry and a short description of the observed objects.

The spectrum of the northeast tidal stream was too faint to be successfully extracted with *apall*. Despite using the largest available slit and the lowest dispersion grism available, the tidal stream proved too faint for useful spectroscopy in 30 min of integration. We obtained, however, well exposed spectra for nine other objects, including knot A, and a less exposed but still useful spectrum of knot B (see Fig. 2). FORS2 was also used to obtain a 400 s Bessel V-band exposure centered on the northeast dog-leg tidal stream (see Fig. 1). The night's seeing (FWHM of unsaturated stars measured on the image) was ≈1″.

3. Results

3.1. Spectroscopy of the condensations in the "dog-leg" tidal stream

The five optical condensations in the northeast tidal stream that were observed spectroscopically with FORS2 are indicated in Fig. 1 and listed in Table 1. Of these, one is a foreground star (Object 9) and two are background galaxies (Objects 6 and 7), with $z \approx 0.1$–0.3. We will not discuss these sources further.

A high quality spectrum was extracted for knot A, and is shown in Fig. 2. The spectrum is notable for a total lack of emission lines ordinarily found in star forming systems like [O III] $\lambda\lambda$ 4959, 5007 Å, Hβ or Hα, in agreement with Arp (1976) and Wehrle et al. (1997). However, these new observations set more stringent limits on Hα emission, with $EW_{\mathrm{H}\alpha} <$ 5 Å . Several narrow hydrogen Balmer absorption lines (Hγ, Hβ, and Hα) are clearly detected, with equivalent widths (measured with IRAF's *splot* tool) of 2.9, 3.8 and 2.3 Å respectively (see Table 2). There is also evidence for a weak G-band (λ 4303 Å) absorption. The most prominent feature in Fig. 2 is a strong break in the continuum level at ≈4400 Å.

We derive synthetic optical colors for knot A using the spectrum in Fig. 2 by numerically integrating over the Johnson-Cousins $UBVRI$ passbands, and find $B - V = 0.8 \pm 0.1$, $B - R = 1.3 \pm 0.1$, $V - R = 0.5 \pm 0.1$ and $V - I = 0.9 \pm 0.1$. Note that these colors are somewhat redder than the colors of the local diffuse jet emission as measured by CAM ($B - R = 0.9 \pm 0.2$). The 1.8σ deviation between our and CAM's measures is not surprising considering the inherent difficulty in measuring the colors of such a low brightness feature, and the fact that CAM performed

[1] knots A & B referred to in this paper correspond to the two optical knots discussed in Wehrle et al. (1997). Our knot A is also the "bright condensation" in jet R1 discussed by CAM (see their Sect. 3 and Table 2).

[2] IRAF is distributed by the National Optical Astronomy Observatories, which are operated by the Association of Universities for Research in Astronomy, under contract with the National Science Foundation.

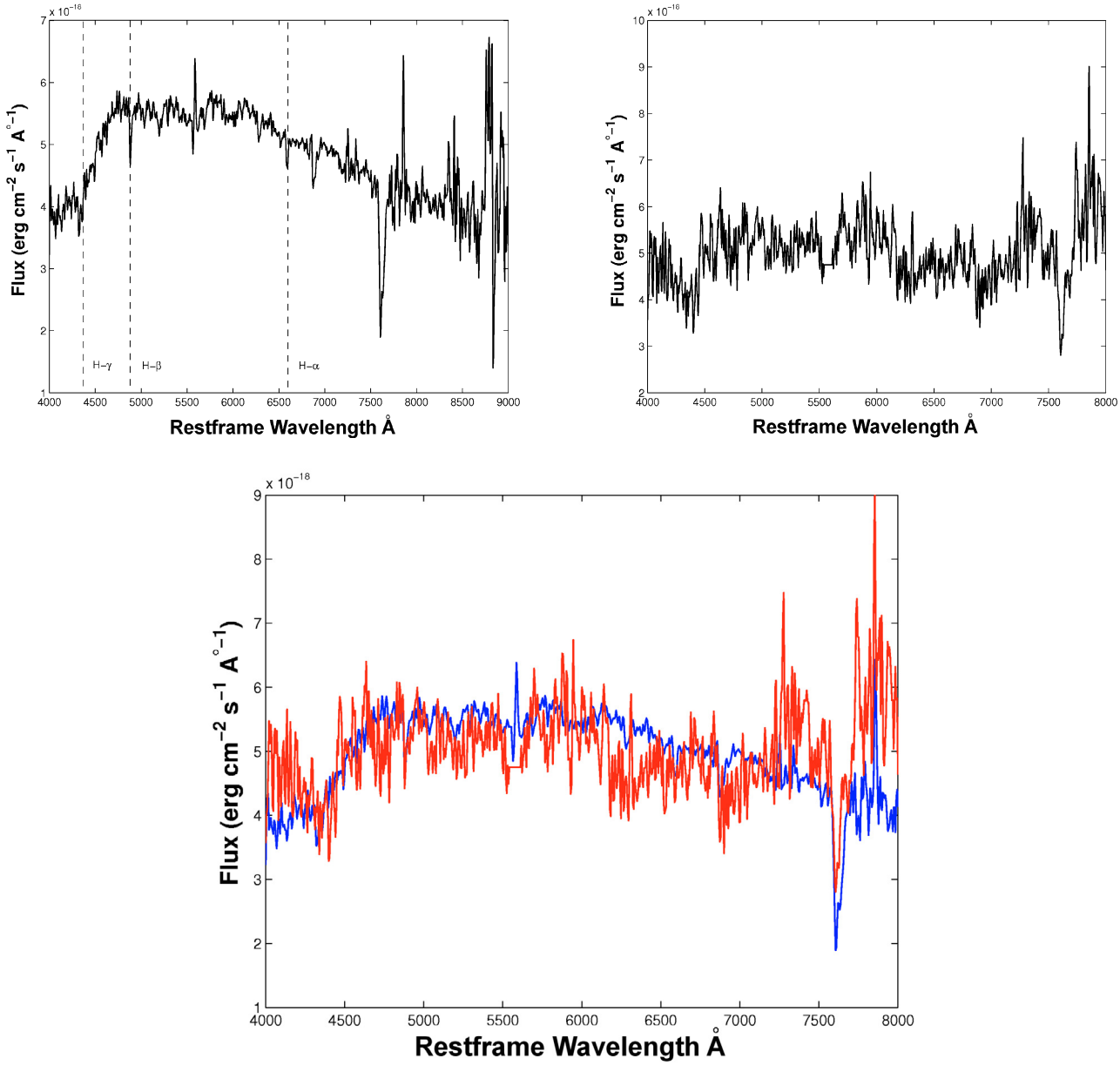

Fig. 2. *Up left:* FORS2 spectrum of knot A. *Up right*: FORS2 spectrum of knot B. *Bottom*: comparison of knot A's spectrum (blue line) vs. knot B's (red line).

those measures more than 20 yr ago, using normal photographic plates.

From the measured wavelengths of absorption lines in knot A's spectrum (see Table 2) we derive a redshift of $z = 0.0043 \pm 0.0001$. This is within $\Delta z = 0.0001$ of NGC 1097's redshift derived using HI and optical emission lines, and shows that knot A is indeed physically associated with the barred spiral galaxy.

As shown in Fig. 2 (upper-right panel) the two features in the spectrum of knot B, being possibly significant above the noise are the break in the continuum level at 4400 Å and the Hβ line at 4882 Å. As is shown in Fig. 2 (bottom panel) the overall continuum shape and the position of these two features match fairly well those of knot A, indicating that their redshifts could be similar. Under the assumption that knot B is at the same redshift distance of knot A, we find moreover that knot B agree very well with the same photometric scaling relations of knot A. This makes it unlikely that knot B is a galaxy with a different absolute magnitude than knot A, placed at a different distance from NGC 1097. We will therefore assume throughout the rest of the article that knot B is physically associated with NGC 1097.

3.2. Surface photometry and morphology of knots A & B

Both knots A & B in the NE tidal stream are easily seen in the FORS2 *V*-band image shown in Fig. 1. We are able to extract new details concerning their morphologies: Knot A shows considerable spherical symmetry, with a bright and compact core and a halo that extends for the full width of the stream (≈15″), while knot B is more diffuse and lacks a central core (see Fig. 3).

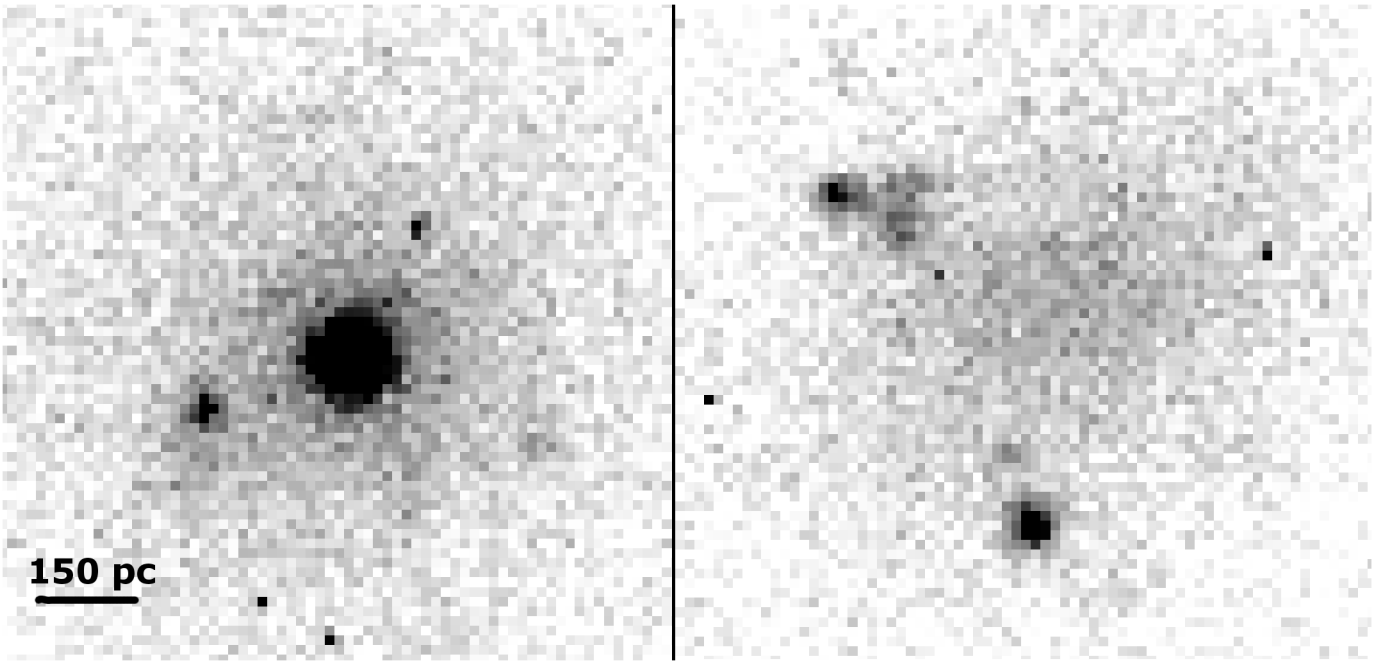

Fig. 3. Closeups (13″ × 13″) from the Bessel V-band image of NGC 1097's dog-leg region (Fig. 1) showing (*left*) knot A and (*right*) knot B. Identical linear stretches are used.

Table 1. Magnitudes of the observed objects: The labels fs, bg, c indicate respectively: "foreground star", "backgroung galaxy", "condensation". The typical rms errors for the magnitudes are 0.1 mag.

Obj. ID	RA	Dec (J2000)	m_v (mag)	Type
1	02:47:00	–30:13:04	21.3	fs
2	02:47:01	–30:12:59	19.9	bg
3	02:46:59	–30:11:55	21.4	fs
4	02:47:01	–30:11:48	21.2	bg
5(knot A)	02:47:00	–30:10:08	19.9	c
6	02:47:04	–30:09:30	20.0	bg
7	02:47:04	–30:09:22	21.5	bg
8(knot. B)	02:47:05	–30:09:07	20.4	c
9	02:47:07	–30:08:38	22.1	fs
10	02:47:12	–30:06:58	23.4	bg
11	02:47:11	–30:06:57	23.6	bg

Table 2. Absorption redshift of knot A: $\lambda_{\rm meas}$ is the measured wavelength, λ_0 is the rest-frame wavelength, z is the measured redshift and Δz is the redshift difference with NGC 1097 ($z = 0.0042$ NED).

Line	$\lambda_{\rm meas}$	λ_0	z	Δz	EW (Å)
H_α	6592.0	6562.8	0.0044	0.0002	2.9
H_β	4882.1	4861.3	0.0043	0.0001	3.8
H_γ	4359.1	4340.5	0.0043	0.0001	2.3

Averaged V-band surface brightness profiles (SBPs) for knots A & B were extracted using the IRAF/STSDAS task *ellipse* and are shown in Fig. 4. A small number of faint and unresolved objects surrounding the nuclei of both knots are apparent in Fig. 3. These were excluded from the SBP extraction using a pixel mask. We fit the SBPs of both knots using the $R^{1/n}$ parameterization of Sérsic (1968), which can be written:

$$\mu(R) = \mu_{\rm e} \exp\left\{-b_n\left[\left(\frac{R}{R_{\rm e}}\right)^{1/n} - 1\right]\right\}, \quad (1)$$

where R is the projected radial distance from the center of the galaxy. This representation is widely used and has the advantage of precisely describing a variety of SBPs, including pure exponential and de Vaucouleurs $R^{1/4}$ laws, i.e., those of both dwarf and luminous elliptical galaxies (Faber & Lin 1983; de Vaucouleurs 1948, 1959). The free parameters of this model are $R_{\rm e}$, $\mu_{\rm e}$ and n, where n describes the shape of the distribution. The coefficient b_n depends on n and can be chosen in such a way that $R_{\rm e}$ and $\mu_{\rm e}$ coincides respectively with the half light radius of the object (i.e. the radius enclosing half of the total flux) and the surface brightness at that radius. As shown by Capaccioli (1987) for $1 < n < 10$ we have $b_n \approx 1.9992n$–0.3271. Since $n < 1$ for our objects, one can question whether this approximation is appropriate. As shown by Graham (2001) the difference between the exact value of $b_n(n)$ and Capaccioli's approximation is about b_n(exact) – b_n(approx) = 0.03 for $n = 0.4$ (knot B). Considering the uncertainties of our fits (RMSE ≈ 0.1) we have neglected such small differences.

The SBPs for knots A & B are shown in Fig. 4, along with the fitted Sérsic model and residuals. The latter are small with no systematics and indicate good fits for both objects. Derived values of n, $R_{\rm e}$, and $\mu_{\rm e}$ and their uncertainties are included in Table 3. Knot A possesses a bright and marginally resolved core that cannot be represented by a Sérsic profile. For this reason we restricted the fitting region to exclude the inner 1.6″, which in Fig. 4 can be seen to correspond to the radius at which the fitted Sérsic profile begins to depart from the data points, and agrees very well with the optical size of the bright core (Fig. 3). Knots A & B have fitted Sérsic exponents $n_A = 0.6 \pm 0.1$ and $n_B = 0.4 \pm 0.1$, and central V-band surface brightnesses (i.e., extrapolating the fitted Sérsic profile to $R = 0$ for knot A) of $\mu_{A,0} = 24.6 \pm 0.2$ mag arcsec^{-2} and $\mu_{B,0} = 25.1 \pm 0.2$ mag arcsec^{-2}.

Accurate half-light radii have been computed for both objects. For knot B, we estimate the half-light radius from the Sérsic model fit to be (see above) $R_{\rm e} = 428 \pm 84$ pc, where we have included contributions from the pixel scale and saturation effects in the uncertainty. Since knot A's core cannot be fit by a

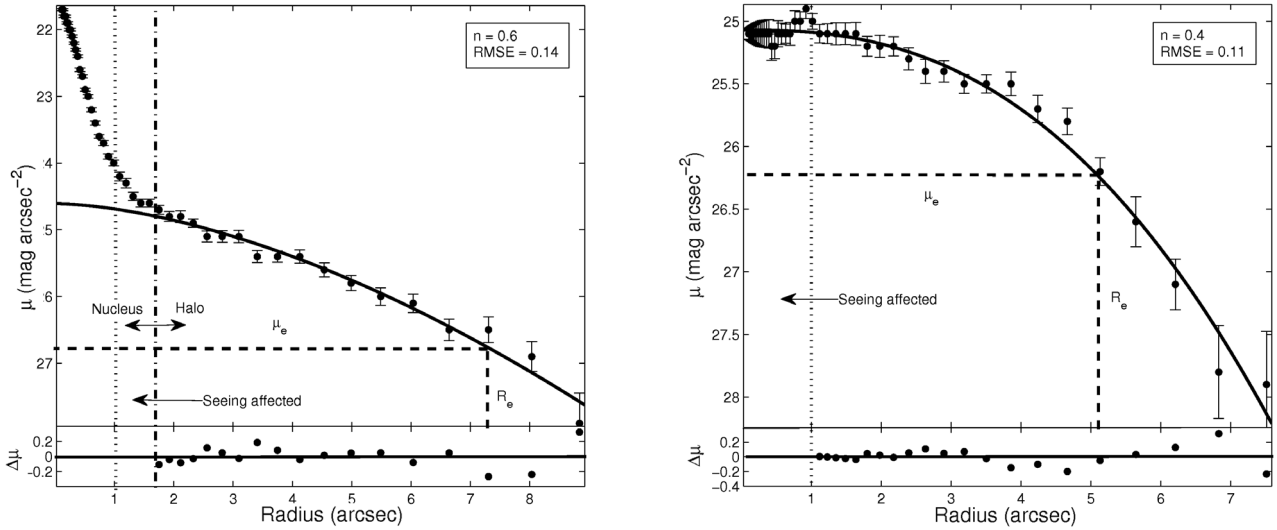

Fig. 4. *Left*: Knot A's surface brightness profile obtained with IRAF's *ellipse* task. The continuos line represent the Sérsic $n = 0.6$ model fit. The dotted line delimits the seeing affected zone, while the dash-dotted line is placed at $R_{\rm core} = 1.6''$. Since the nucleus is only partially resolved, data points below $R_{\rm core}$ have been excluded from the fit. *Right*: same as previous, but for knot B. In this case the Sérsic index is $n = 0.4$ and data points below $1''$ have been excluded from the fit.

Sérsic profile, we estimate an empirical half-light radius using the *ellipse* output to calculate the radius at which the total flux drops by half. In this way we obtain $R_{\rm e} = 336 \pm 84$ pc.

Integrated apparent V-band magnitudes were determined to be $m_V = 19.9 \pm 0.1$ mag and $m_V = 20.4 \pm 0.1$ mag for knots A & B respectively, which correspond to absolute magnitudes of $M_V = -11.2 \pm 0.1$ and $M_V = -10.8 \pm 0.1$ at the adopted distance of NGC 1097. Assuming $M_{\odot,V} = 4.82$ (Bell & de Jong 2001), these translate into V-band luminosities of $L_V = 2.6 \times 10^6\ L_{\odot,V}$ for knot A and $L_V = 1.6 \times 10^6\ L_{\odot,V}$ for knot B. We also estimate m_V, M_V, and L_V for knot A's core using a circular aperture of radius $3 \times R_{\rm core}$, and find $m_V = 21.4 \pm 0.1$ mag, $M_V = -9.8 \pm 0.1$ and $L_V = 6.9 \times 10^5\ L_{\odot,V}$.

Dwarf galaxies subject to ongoing tidal perturbations may show surface brightness "breaks" or other irregularities in their outer isophotes (Peñarrubia et al. 2009). We are however unable to detect such irregularities in our surface brightness profiles (see Fig. 4).

This however does not necessarily imply that the knots are not being tidally stripped, since as shown by Peñarrubia et al. (2009) such "bumps" in the isophotes are essentially transient features that quickly drift in the outer region of the SBPs, where the S/N may be too low to give any useful information. Their eventual detection is therefore related to the time of the observation, and strongly depends on the orbital parameters of the tidally-disrupting object. Moreover, it is likely that the spatial resolution of our SBPs is simply insufficient to reveal these "bumps": our objects have in fact a very small angular extension if compared to Local Group (LG) dwarfs. It is however difficult to estimate the expected amplitude of these irregularities without knowing the orbit of the objects and their internal kinematics.

3.3. Stellar population

The resolution of knot A's spectrum ($\delta\lambda = 19$ Å at 5000 Å) is too low to accurately estimate metal abundances from spectral line indices. An estimate of its metallicity would be nonetheless useful to help constrain its nature.

In order to extract more information regarding knot A's stellar population, we cross-correlated its spectrum with that of 40 galactic GCs from the library in Schiavon et al. (2005), which covers a wide range of metallicities from –2 dex to solar abundance. We degraded the spectral resolution of the 40 galactic GCs to match that of knot A's spectrum, and used the IRAF task *fxcor* for cross-correlation.

With this method we find a linear relation between the cross correlation amplitudes of knot A (plus two test GCs) and the [Fe/H] ratios of the library's GCs (see Fig. 5). This is reasonable considering that for evolved stellar populations, the [Fe/H] ratio should play an important role in determining spectral differences. This implies that the [Fe/H] ratio of knot A can be estimated – at least qualitatively – using this cross correlation technique.

The results of the left panel of Fig. 5 imply an [Fe/H] ratio >–1.0 dex for knot A. The analogous plots in the middle and right panel for a metal-poor and a metal-rich GC confirm the validity of this approach, since the slope of the cross-correlation amplitude vs. [Fe/H] is, as expected, negative for the metal-poor and positive for the metal-rich GCs.

Figure 6 confirms the results of Fig. 5 by comparing knot A's spectrum with the two GCs with highest and lowest cross-correlation amplitudes. The match is very good for the GC NGC 6388, which is of intermediate metallicity ([Fe/H] = –0.7 dex), and shows a clear discrepancy for NGC 1904, which has a lower metallicity ([Fe/H] = –1.5 dex). Since NGC 6388 has an integrated spectral type of G2, while NGC 1904 has type F4/5 (Harris et al. 1996), we can state that the light emitted by knot A's is most likely dominated by G-type stars, in agreement with CAM.

While it is true that this method does not precisely determine the [Fe/H] ratio, the results shown in Figs. 5 and 6 indicate (at least qualitatively) that knot A's metal abundances are higher than LG dwarf spheroidals of similar luminosity (e.g., [Fe/H] = –1.5 dex; Mateo 1998). It has been shown however, that dSph galaxies belonging to different clusters of galaxies may show sensible differences in their metallicity-luminosity relation, if compared with LG dwarves (Lianou et al. 2010).

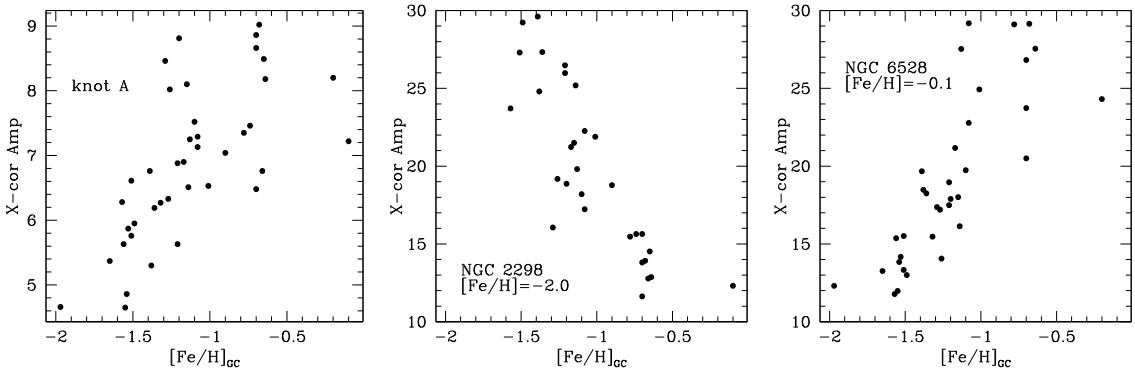

Fig. 5. *Left*: Knot A's cross correlation amplitude as a function of metallicity for galactic GCs from Schiavon (2005). The rough linear relation of positive slope, indicates that our spectrum is better fit by metal-rich than metal-poor GCs (see the text and next figure for details). *Center, right*: the same as left for two Galactic GCs from the same library, whose metallicity has been estimated with HR spectroscopy. As expected, the metal poor GC NGC 2298 correlates better with metal poor GCs while the metal rich GC NGC 6528 correlates best with metal rich GCs.

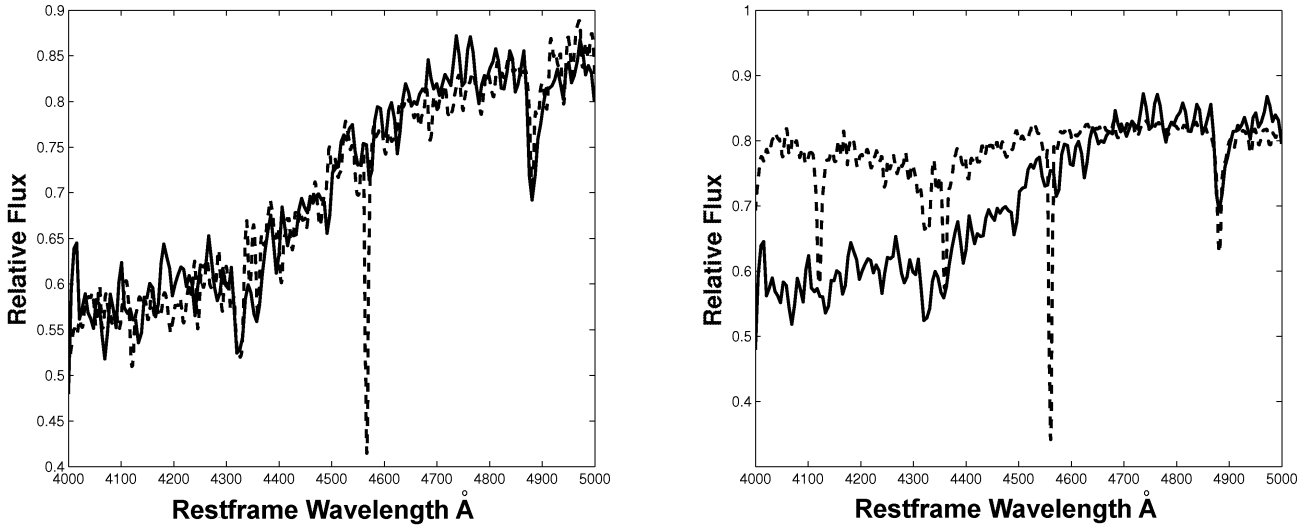

Fig. 6. *Left:* Comparison between knot A's spectrum (continuous line) and the best correlating GC from Schiavon (2005) (dashed line, cross correlation amplitude 9), which is the intermediate metallicity GC NGC 6388. *Right*: the same as left with the worst correlating GC from Schiavon et al. (2005) (cross correlation amplitude 4.5), which is NGC 1904. The two plots show that knot A's spectrum correlates best with intermediate to high metallicity GCs like NGC 6388 ([Fe/H] = −0.7), rather than with metal poor ones like NGC 1904 ([Fe/H] = −1.5).

Table 3. Summary of measured and estimated (E) parameters for knots A & B.

Parameter name	knot A	knot B
Redshift	$z = 0.0042 \pm 0.0001$	=
Heliocentric distance	$D = 17 \pm 2$ Mpc	=
Integrated V magnitude	$m_v = 19.9 \pm 0.1$ mag	$m_v = 20.4 \pm 0.1$ mag
Nucleus V magnitude	$m_{v_{\rm nuc}} = 21.4 \pm 0.1$ mag	–
Absolute magnitude	$M_V = -11.2 \pm 0.1$ mag	$M_V = -10.8 \pm 0.1$ mag
Half light radius	$R_{\rm e} = 336 \pm 84$ pc	$R_{\rm e} = 482 \pm 84$ pc
Central surface brightness	$\mu_{A,0} = 24.6 \pm 0.2$ mag arcsec^{-2}	$\mu_{B,0} = 25.1 \pm 0.2$ mag arcsec^{-2}
Sérsic index	$n = 0.6 \pm 0.1$	$n = 0.4 \pm 0.1$
Predominant stellar type	G	=
Stellar mass	$M_* \approx 6 \times 10^6\ M_\odot$	$M_* \approx 4 \times 10^6\ M_\odot$

4. Discussion

4.1. Are the knots dwarf spheroidal galaxies?

We have shown that knot A's optical spectrum and total luminosity matches well that of intermediate to metal rich and massive GCs like 47 Tucanae and Mayall I. However, the size of knot A ($R_{\rm e} = 337 \pm 84$ pc) is abundantly beyond those of ordinary GCs, the vast majority of which possess $R_{\rm e} < 10$ pc (cf. Mackey & van den Bergh 2005). In terms of size both knots A & B are similar to LG dSph satellite galaxies of comparable luminosity (Mateo 1998). It has been established that dSph galaxies and GCs occupy different positions in a plot of half-light radius versus $M_{\rm V}$. Large GCs in fact obey a well defined relation, in the sense that larger GCs are also fainter ($\log[R_{50}] = 0.25\ M_{\rm V} + 2.5$; Mackey & van den Bergh 2005; though Van den Bergh 2008 discusses

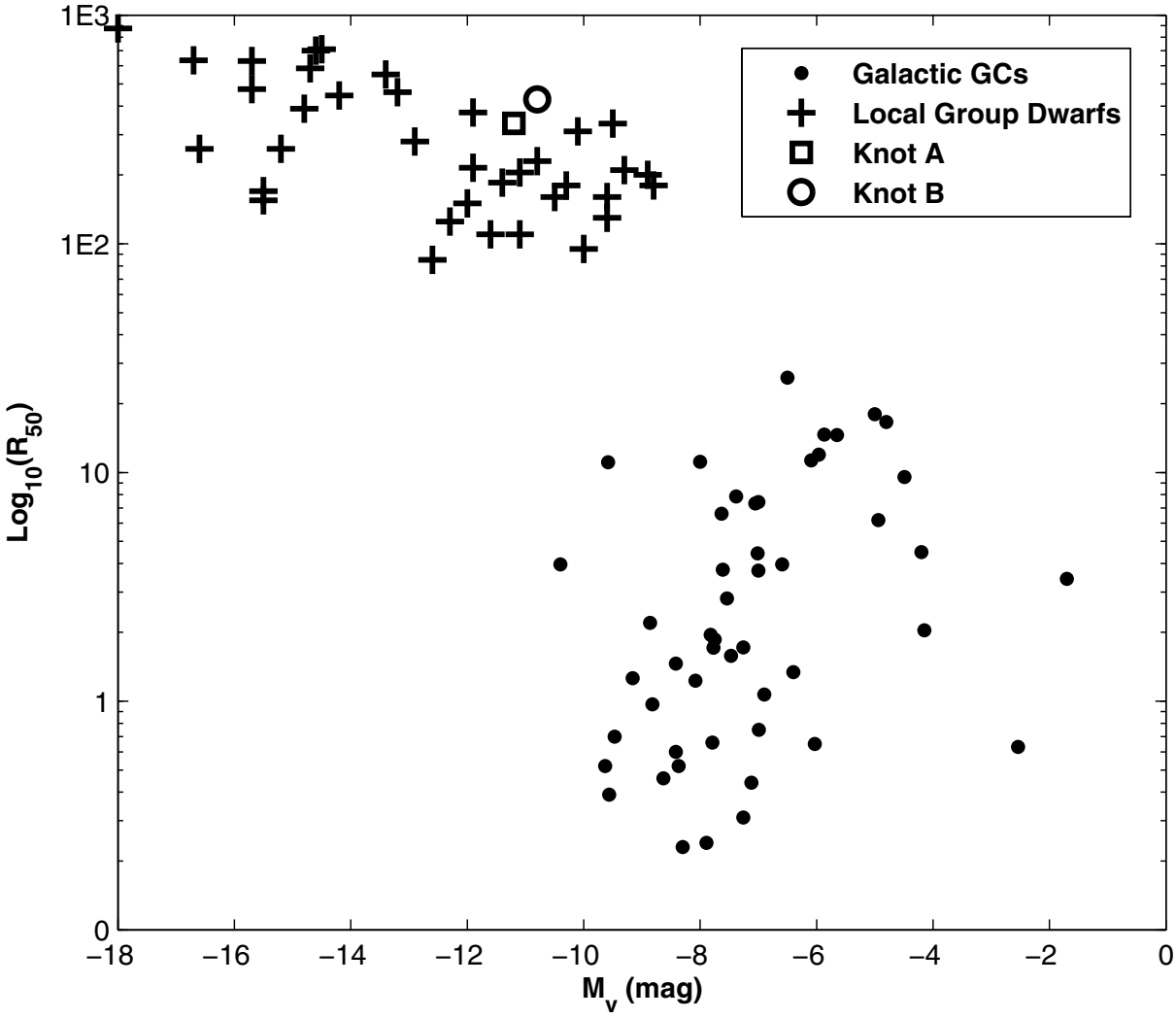

Fig. 7. Absolute magnitudes vs half light radii for local group dwarfs from (Mateo 1998), Galactic globular clusters (Webbink 1985) and the two knots.

shortcomings of this diagnostic). Knots A & B are well above this line trend (they are much larger for their optical luminosity than GCs) (see Fig. 7). Instead, the knots agree very well with the M_v−$\mu_{0,V}$ relation for LG and Hydra/Centaurus dwarves (Misgeld et al. 2008, 2009). They found that typical dSph galaxies follow the relation (cf. Misgeld et al. 2009):

$$\mu_{0,V}* = 0.57[\pm0.07] * M_V + 30.90[\pm0.87]. \quad (2)$$

Substituting $M_V = -11.2 \pm 0.1$ for knot A and $M_V = -10.8 \pm 0.1$ for knot B, we obtain $\mu_{0,A}* = 24.6 \pm 0.085$ mag arcsec^{-2} and $\mu_{0,B}* = 24.74 \pm 0.085$ mag arcsec^{-2}, which matches very well our measured central surface brightnesses (see Table 3). Our Sérsic indexes of $n_A = 0.6 \pm 0.1$ and $n_B = 0.4 \pm 0.1$ also agree very well with the typical values for Hydra/Centaurus dwarfs with a $M_v \approx -11$ that is (cf. Misgeld et al. 2009) $n = 0.5 \pm 0.1$.

In terms of stellar population (old GC-like stellar population with no signs of ongoing SF and a peculiar lack of HI), stellar mass ($M_* \approx 6 \times 10^6\ M_\odot$ for knot A and $M_* \approx 4 \times 10^6\ M_\odot$ for knot B), central surface brightness and Sérsic index (see above), M_v vs R_{50} (see Fig. 7) our knots closely resemble ordinary dSph galaxies, as defined in Grebel et al. (2003) and Mateo (1998).

4.2. Structure and composition of the stellar stream

The stellar stream itself was too faint for quantitative spectroscopy. From our sky-substracted V-band exposure however (see Fig. 1), we could measure the mean surface brightness of the stream (measured over ten different apertures a long the "dog-leg"). The value that we obtained is $\mu_V = 26.5 \pm 0.2$ mag/arcsec^2. After measuring the mean SB of the stream using the standard IRAF tools, authors PG and SM independently measured the size of the stream, by subdividing it in small rectangular apertures. The value found is 8400 ± 100 arcsec^2. From the measurement of the stream's mean surface brightness and its area, we have calculated its integrated V magnitude to be $m_V = 16.6 \pm 0.2$ mag. At the distance of NGC 1097 this corresponds to an absolute magnitude of $M_V = -14.5 \pm 0.35$ mag.

Useful hints about the composition of the tidal stream can be found in earlier studies (CAM, HW, Wehrle et al. 1997). Using multiband photometry of the tidal stream (obtained in a region slightly south-western than knot A) CAM suggested that the SED of the "dog-leg" feature is compatible with G-type stars. They also found that the colors of the stream and knot A are

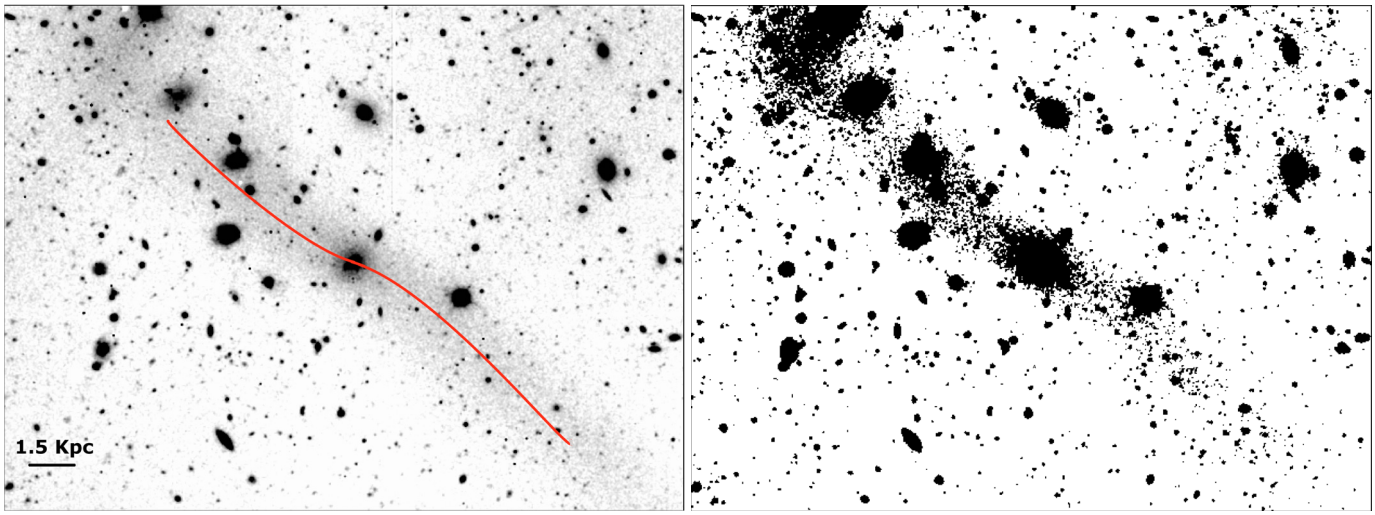

Fig. 8. *Left*: in this ehnanced version of Fig. 1 (3″ Gaussian smoothing, logarithmic scaling of intensities) we show how the stream forms an "S" shaped inflection in correspondence of knot A. *Right*: at higher contrast the elliptical overdensity within the stream is clearly centered on knot A's position. Both features are typical for tidally disrupting systems.

similar within the photometric uncertainties ($B - R_{\rm str.} = 0.55 \pm 0.36$, $B - R_A = 0.9 \pm 0.18$). This last point agrees with the conclusions of Wehrle et al. (1997). In their paper they measured the B/V count ratio longitudinally and transversally along the tidal stream (see their Fig. 8), and concluded: "The color (along the tidal stream) is constant within the errors, including both prominent condensations". Both studies came to the conclusion that the stellar stream is composed of stars near G-type, and that the stream and the knots have the same color. With our FORS2 spectra, we independently showed that also knot A is predominantly composed of stars near G-type. This suggests that the knots and the tidal stream are both composed of the same stellar material.

A morphological analysis of the tidal stream indicates that knot A is currently being tidally stripped, populating the "dog-leg" tidal stream with stars. As shown in Fig. 8 (left), the tidal stream shows a slight but significant "S" shaped inflection coincident with the position of knot A. In Fig. 8 (right), we show moreover the elliptical overdensity of stars at knot A's position. These morphological features are typical for tidally disrupting systems (Forbes et al. 2003; Martínez-Delgado et al. 2008, 2010).

If knot A is the only progenitor of the stellar stream, before the encounter with NGC 1097, knot A should have been a dwarf galaxy of at least $M_V = -14.5 \pm 0.35$ mag. This means that knot A has lost at least the 95% of its stars during the encounter with NGC 1097. This is in agreement with the n-body simulations performed by HW.

4.3. How did the knots form?

The alignment of knots A & B with the "dog-leg" tidal stream suggests that these two objects are probably correlated in phase-space. Such a perfect alignment along the same stream would be in fact very unlikely for independently infalling CDM-Subhalos.

A possible explaination to the phase-space correlation problem of Milky Way satellites (Kroupa et al. 2005; Metz et al. 2009a), has been proposed in terms of a "group infall" of subhalos (Li & Helmi 2008; D'Onghia & Lake 2008; D'Onghia et al. 2009). Alternately, dwarf galaxies may form along dark matter filaments (Ricotti et al. 2008). It is, however, still unclear if these mechanisms can efficiently explain the observed distribution of satellite galaxies around the Milky Way and Andromeda (for recent criticism see: Metz et al. 2009b,a).

The alignment of knots A & B with the stream is instead reminescent of the situation in the Milky Way, where the disk-of-satellites is approximately aligned with the Magellanic Stream (Metz et al. 2009b). This may suggest that the satellite galaxies of NGC 1097 may also be interpreted as being old tidal dwarf galaxies (Zwicky 1956; Lynden-Bell 1983; Okazaki & Taniguchi 2000).

However, a definitive interpretation awaits further study, in particular, we need to examine both knots' internal kinematics, and whether NGC 1097 has additional dSph satellite galaxies. The deep implications for fundamental physics of objects such as knots A & B being tidal dwarf galaxies are discussed in Kroupa et al. (2010).

5. Conclusions

We have shown that the two optical "knots" along NGC 1097's tidal stream share most of their observable properties with ordinary dwarf spheroidal galaxies (dSphs). From the measured redshifts we show that knot A (and very likely knot B) are associated with the tidal stream. The spectral light distribution of these dSphs is most consistent with that of intermediate to metal-rich Galactic GCs (see Figs. 6, 7).

These new observations set more stringent limits for Hα emission of the tidal stream, with $EW_{\rm H\alpha} < 5$ Å.

Our new observations, togheter with the results from former studies (Carter et al. 1984; Wehrle et al. 1997; Higdon & Wallin 2003), indicate that knot A is composed of the same stellar material as the tidal stream. Moreover, a morphological analysis of the tidal stream reveals clear signs of ongoing tidal stripping (see Fig. 8). Based on this evidence we conclude that very likely the stellar stream is populated by stars drawn out from knot A.

The presence of ongoing tidal stripping is incompatible with knot A being surrounded at present by a massive CDM halo (Peñarrubia et al. 2008, 2009).

Acknowledgements. We wish to thank Halton C. Arp (MPA Garching) and Gero Rupprecht (ESO Garching), E.M. Burbidge and V. Jukkarinen (CASS San Diego) for their useful comments. We wish to extend a special word

of thanks to Martino Romaniello (ESO Garching), Dieter Horns and Andrea Santangelo (IAAT Tuebingen) for their help during the preliminary stages of this paper.

References

Arp, H. 1976, ApJ, 207L,147A
Appenzeller, I., Fricke, K., Frütig, W., et al. 1998, The Messenger, 94, 1
Bekki, K., Couch, W. J., Drinkwater, M. J., & Shioya, Y. 2003a, MNRAS, 344, 399
Bekki, K., Forbes, D. A., Beasley, M. A., & Couch, W. J. 2003b, MNRAS, 344, 1334
Bell, E. F., & de Jong, R. S. 2001, ApJ, 550, 212
Bruzual, G., & Charlot, S. 2003, MNRAS, 344, 1000B
Carter, D., Allen, D. A., & Malin, D. F. 1984, MNRAS, 211, 707
Capaccioli, M. 1987 in Structure and Dynamics of Elliptical Galaxies, ed. P. T. de Zeeuw (Dordrecht: Reidel), IAU Symp., 127, 47
Dekel, A., & Silk, J. 1986 ApJ, 303, 39
D'Onghia, E., & Lake, G. 2008, ApJ, 686, L61
D'Onghia, E., Besla, G., Cox, T. J., & Hernquist, L. 2009, Nature, 460, 605
Duc, P. A., & Mirabel, I. F. 1994, A&A, 289, 83
de Vancouleurs, G. 1948, Ann. d'Astrophysique, 11, 247
de Vaucouleurs, G. 1959, Handb. Phys., 53, 275
Drinkwater, M. J., Jones, J. B., Gregg, M. D., & Phillipps, S. 2000, PASA, 17, 227
Faber, S. M., & Lin, D. N. C. 1983, ApJ, 266L, 17F
Fellhauer, M., & Kroupa, P. 2002, MNRAS, 330, 642
Fellhauer, M., & Kroupa, P. 2005, MNRAS, 359, 223
Forbes, D., Beasley, M. A., Bekki, K., Brodie, J. P., & Strader, J. 2003, Science, 301, 1217F
Genzel, R. et al. 2006, Nature, 442, 17
Graham, A. W. 2001, AJ, 121, 820
Graham, A. W., & Guzman, R. 2003, ApJ, 125, 2936
Gratton, R. G., et al. 2003, A&A, 408, 592
Grebel, E. K., Gallagher, J. S., III, & Harbeck, D. 2003, AJ, 125, 1926
Harris, W. E. 1996, AJ, 112, 1487
Hasegan, M., Jordán, A., Côté, P., et al. 2005, ApJ, 627, 203
Hibbard, J. E., Guhathakurta, P., van Gorkom, J. H., & Schweizer, F. 1994, AJ, 107, 67
Higdon, J. L., & Wallin, J. F. 2003, ApJ, 585, 281 (HW)
Higdon, S. J., Higdon, J. L., & Marshall, J. 2006, ApJ, 640, 768
Hilker, M., Infante, L., & Richtler, T. 1999, A&AS, 138, 55
Hilker, M., Infante, L., Vieira, G., Kissler-Patig, M., & Richtler, T. 1999, A&AS, 134, 75
Hilker, M., Kissler-Patig, M., Richtler, T., Infante, L., & Quintana, H. 1999, A&AS, 134, 59
Kissler-Patig, M., Jordan, A., & Bastian, N. 2006, A&A, 448, 1031
Koribalski, B., Staveley-Smith, L., Kilborn, V. A., et al. 2004, AJ, 128, 16
Kormendy, J., Fisher, D. B., Cornell, M. E., & Bender, R. 2009, ApJS, 182, 216
Kroupa, P. 1997, New Astron., 2, 139, 164
Kroupa, P., Theis, C., & Boily C. M. 2005, A&A, 2, 431, 517K
Kroupa, P., et al. 2010, A&A, in press
Lasker, B. M., Sturch, C. R., McLean, B. J., et al. 1990, AJ, 99, 2019
Lorre, J., J. 1978, ApJ, 222, 99
Li, Y., & Helmi, A. 2008 MNRAS, 385, 1365
Lianou, S., Grebel, E. K., & Koch, A. 2010 A&A, in press
Lynden-Bell, D., & Lynden-Bell, R. M. 1995, MNRAS, 275, 429
Mackey, A. D., & van den Bergh, S. 2005, MNRAS, 360, 631
Maraston, C., Bastian, N., Saglia, R. P., et al. 2004, A&A, 416, 467
Martinez-Delgado, D., Jay Gabany, R., Crawford, K., et al. 2010, ApJL, submitted [arXiv:1003.4860]
Martínez-Delgado, D., Peñarrubia, J., Gabany, R. J., et al. 2008, ApJ, 689, 184M
Mateo, M. 1998, ARA&A, 435, 506
Mathewson, D., & Ford, V. 1996, ApJS, 107, 97
Metz, M., & Kroupa, P. 2007 MNRAS, 376, 387
Metz, M., Kroupa, P., & Jerjen, H. 2009a, MNRAS, 394, 2223
Metz, M., Kroupa, P., Theis, C., Hensler, G., & Jerjen, H. 2009b, ApJ, 697, 269
Meylan, G., Mayor, M., Duquennoy, A., & Dubath, P. 1995, A&A, 303, 761
Meylan, G., Sarajedini, A., Jablonka, P., et al. 2001, ApJ, 122, 830
Mieske, S., et al. 2006, ApJ, 131, 2242
Mirabel, I. F., Dottori, H., & Lutz, D. 1992, A&A, 256, L19
Misgeld, I., Hilker, M., & Mieske, S. 2008, A&A, 486, 697
Misgeld, I., Hilker, M., & Mieske, S. 2009, A&A, 496, 683
Monet, D. G., Levine, S. E., Canzian, B., et al. 2003, AJ, 125, 984
Meylan, G., & Mayor, M. 1986, A&A, 166, 122
Okazaki, T., & Taniguchi, Y. 2000 ApJ, 543, 149
Patat, F. 2003, From twilight to highlight: the physics of Supernovae, ed. W. Hillebrandt, & B. Leibundgut (Springer), 321
Peñarrubia, J., McConnachie, A. W., & Navarro, J. F. 2008, ApJ, 673, 226
Peñarrubia, J., Navarro, J. F., McConnachie, A. W., & Martin, N. F. 2009, ApJ, 698, 222
Phillips, S., Drinkwater, M. J., Gregg, M. D., & Jones, J. B. 2001, ApJ, 560, 201
Prieto, M., Maciejewski, W., & Reunanen, J. 2005, AJ, 130, 1472
Ricotti, M., Gnedin, N. Y., & Shull, J. M. 2008, ApJ, 685, 21
Scarpa, R. 2006, unpublished [arXiv:astro-ph/0504051]
Schweizer, F. 1982, ApJ, 252, 455
Schiavon, R. P., Rose, J. A., Courteau, S., & MacArthur, L. A. 2005, ApJS, 160, 163
Sèrsic, J. L. 1968, Atlas de galaxias australes (Cordoba, Argentina: Observatorio Astronomico)
Spergel, N. D., Verde, L., Peiris, H. V., et al. 2003, ApJS, 148, 175
Storchi-Bergmann, T., Nemmen, R. S., Spinelli, P. F., et al. 2005, ApJ, 624, 13S
Webbink, R. F. 1985, Dynamics of Star Clusters, ed. J. Goedman, & P. Hut, IAU Symp., 113, 541
Wehrle, A. E., Keel, W. C., & Jones, D. L. 1997, AJ, 114, 115
Wolstencroft, R. D., Tully, R. B., & Perley, R. A. 1984, MNRAS, 207, 889
Knierman, K. A., Gallagher, S. C., Charlton, J. C., et al. 2003, AJ, 126, 1227
Vazdekis, A. 1999, ApJ, 513, 224
Zwicky, F. 1956, Ergenisse Exakten Naturwissenschaften, 29, 344